Copy No. _____

Defence Research and Development Canada
Recherche et développement pour la défense Canada

DEFENCE R&D DÉFENSE

Bead on Plate Temper Pass Study

Thermal and Microhardness Study

Christopher Bayley
Shona McLaughlin

Defence R&D Canada – Atlantic

Technical Memorandum
DRDC Atlantic TM 2009-215
September 2009

Canada

This page intentionally left blank.

Bead on Plate Temper Pass Study

Thermal and Microhardness Study

Christopher Bayley
Shona McLaughlin

Defence R&D Canada – Atlantic

Technical Memorandum
DRDC Atlantic TM 2009-215
September 2009

Principal Author

Original signed by Christopher Bayley

Christopher Bayley

Group Leader / Corrosion and Materials

Approved by

Original signed by Terry Foster

Terry Foster

Section Head / DLP

Approved for release by

Original signed by Ron Kuwahara for

Calvin Hyatt

Chair DRP

Abstract

During multiple pass welding, subsequent welding passes provide the heat required to effectively temper underlying welds and their heat affected zones. In low alloy quenched and tempered steels, high cooling rates associated with the welding thermal cycle lead to high hardness phases such as martensite in the heat affected zone. This study measures the cause – cooling rate, and effect – hardness associated shielded manual arc weld beads deposited on a low alloy quenched and tempered steel. The welds were deposited on a fully instrumented panel which had a series of thermocouples positioned along the weld path and were used to validate analytical peak temperature and cooling rate expressions. Following welding, metallurgical analyses including micro-hardness maps revealed the microstructural evolution during subsequent welding passes. The hardness and metallurgical survey indicated that tempering is most effective for locations which have a peak temperature less than the lower critical A_{C1} below which the ferrite to austenite transformation is suppressed and is located adjacent to the visible heat affected zone. This knowledge can be used to develop effective weld tempering strategies required to reduce the prevalence of hard (i.e. brittle) microstructural phases.

Résumé

Lors du procédé de soudage à passes multiples, les passes de rechargement subséquentes fournissent la chaleur nécessaire pour durcir efficacement par revenu les soudures sous-jacentes et leurs zones thermiquement affectées. Dans le cas d'aciers faiblement alliés trempés et revenus, les vitesses de refroidissement élevées associées au cycle thermique du procédé de soudage entraînent la formation de phases d'une grande dureté, par exemple de la martensite, dans la zone thermiquement affectée. Dans le cadre de l'étude faisant l'objet du présent rapport, on a mesuré des paramètres qui représentent respectivement la cause, soit la vitesse de refroidissement, et l'effet, à savoir la dureté associée aux cordons de soudure déposés, par soudage manuel à l'arc sous atmosphère de protection, sur un acier faiblement allié trempé et revenu. Les soudures ont été exécutées sur un panneau à instrumentation complète comprenant une série de thermocouples situés le long de l'axe de soudage et elles ont servi à valider les valeurs obtenues par analyse de la température de pointe et de la vitesse de refroidissement. Les résultats d'analyses métallurgiques effectuées après le soudage, dont des cartes de répartition de la microdureté, permettent de mettre en évidence l'évolution de la microstructure au cours des passes de rechargement subséquentes. Les valeurs de dureté mesurées et les résultats des analyses métallurgiques indiquent que le revenu a un effet maximal dans les zones qui présentent une température de pointe moins élevée que la température critique inférieure A_{C1}, sous laquelle la transformation de ferrite en austénite est inhibée, et qui sont adjacentes à la zone thermiquement affectée visible. Ces connaissances peuvent faciliter l'élaboration de stratégies efficaces, basées sur le revenu par soudage, qui sont nécessaires pour réduire la fréquence de phases de microstructures dures (c'est-à-dire cassantes).

This page intentionally left blank.

Executive summary

Bead on Plate Temper Pass Study: Thermal and Microhardness Study

Bayley, C.; McLaughlin, S.; DRDC Atlantic TM 2009-215; Defence R&D Canada – Atlantic; September 2009.

Introduction or background: Weld tempering is a well established process which is used to anneal hard martensitic phases from previous welding passes. These martensite phases develop under even the slowest cooling rates in low-alloy quench and tempered steels such as Q1N (HY-80) used in the construction of submarine pressure hulls. While the martensitic phase is hard, it has limited ductility and poor toughness and therefore is considered to be undesirable. Weld tempering provides the necessary driving force to anneal the martensite in order to restore its ductility and toughness and is achieved through the thermal profile of correctly located welding passes.

Results: Both the cause and effects of the high hardness and tempering are examined for a series of bead on plate welding passes deposited on HY-80 steel. Welding beads with three different heat inputs ranging from 776 to 1380 J/mm were specified in order to obtain substantially different thermal conditions. By staggering the start position, this study examined the microstructural evolution which occurred with subsequent weld passes. The measured weld thermal data were found to agree very well with classical analytical peak temperature and cooling rate expressions. Microhardness measurements acquired on a 500×500 μm grid were used to establish hardness maps which graphically represent the hardness of a weld cross section. These maps are found to provide an intuitive means to assess the evolution of the hardness and a way of visualizing the effects of the tempering process.

Significance: By being able to visualize the hardness maps of multi-pass welds, the effectiveness that the weld heat input has on the tempering is clearly and intuitively displayed. Combining these plots with knowledge of the peak temperature and cooling rates, the region of material which experiences the required peak temperature is found to lie below the lower critical reheating temperature associated with the ferrite to austenite transformation. This knowledge allows welding engineers the ability to customize their welding procedures to include appropriately located welding temper passes, and hence avoid partially tempered regions as found on HMCS VICTORIA.

Future plans: The current study was restricted to a limited number of weld beads which is neither representative of weld build-up nor butt welding. Further studies which examine the effect of tempering on greater areas are required and underway.

Sommaire

Bead on Plate Temper Pass Study: Thermal and Microhardness Study

Bayley, C.; McLaughlin, S.; DRDC Atlantic TM 2009-215; Defence R&D Canada – Atlantic; September 2009.

Introduction : Le revenu par soudage constitue un procédé bien établi qui permet d'effectuer le recuit de phases martensitiques dures résultant de passes de rechargement antérieures. Ces phases martensitiques se forment, même à de très faibles vitesses de refroidissement, dans les aciers faiblement alliés trempés et revenus tels que l'acier Q1N (HY-80) utilisé pour construire des coques épaisses de sous-marins. Malgré la dureté de la phase martensitique, celle-ci possède une ductilité restreinte et une piètre ténacité, et la présence de cette phase est donc considérée comme non souhaitable. Le revenu par soudage fournit l'énergie cruciale pour réaliser le recuit de la martensite et, ultérieurement, en restaurer la ductilité et la ténacité; le procédé est exécuté par le biais du profil thermique de passes de rechargement effectuées en des endroits adéquats particuliers.

Résultats : On a examiné des paramètres qui représentent respectivement la cause et les effets de la dureté élevée et du revenu, pour une série de cordons de soudure déposés au moyen de passes de rechargement sur plaque sur de l'acier de nuance HY-80. Selon les spécifications, trois cordons de soudure ont été produits avec des apports de chaleur distincts variant entre 776 et 1380 J/mm, afin d'obtenir des conditions thermiques très différentes. Le décalage du point de départ du cordon a permis d'étudier l'évolution de la microstructure au cours des passes de rechargement subséquentes. Les résultats indiquent qu'il y a un très bon accord entre les données de nature thermique de la soudure et les valeurs obtenues par analyse classique de la température de pointe et de la vitesse de refroidissement. Des mesures de microdureté enregistrées sur une grille de 500 micromètres sur 500 micromètres ont été utilisées pour établir des cartes de répartition de la microdureté, lesquelles constituent une représentation graphique de la dureté de le section transversale d'une soudure. Des cartes de ce type constituent à la fois une méthode d'analyse intuitive permettant d'évaluer l'évolution de la dureté, ainsi qu'un outil de visualisation des effets du traitement de revenu.

Portée : La capacité de visualiser des cartes de répartition de la dureté de soudures produites par soudage à passes multiples permet d'établir, de manière claire et intuitive, le degré d'efficacité de l'apport thermique de la soudure sur le processus de revenu. En combinant les données de ces schémas aux connaissances relatives à la température de pointe et aux vitesses de refroidissement, il est possible d'établir que la température des zones du matériau qui présentent la température de pointe requise, est moins élevée que la température critique inférieure de réchauffage, laquelle est associée à la transformation de la ferrite en austénite. Ces connaissances permettent maintenant aux ingénieurs en soudage de personnaliser les procédés de soudage qu'ils emploient afin d'y intégrer l'exécution de passes de rechargement en des endroits adéquats particuliers, ce qui évitera la formation de zones ayant subi un revenu partiel comme celles observées sur le NCSM VICTORIA.

Recherches futures : La portée de l'étude actuelle se limitait à l'examen d'un nombre restreint de cordons de soudure qui n'étaient pas représentatifs de soudures superposées ou de soudures en bout. Il faudra réaliser des études supplémentaires sur les effets du revenu sur des zones de plus grande taille, et ce, même si de telles études sont déjà en cours.

This page intentionally left blank.

Table of contents

List of figures

List of tables

Acknowledgements

This work was made possible with the support of the welding officer and welding shop at Fleet Maintenance Facility Cape Breton along with technical support from the staff at the Dockyard Laboratory Pacific. In particular the efforts made by Mr Joel Higgins for the instrumentation and thermal data collection along with endless metallographic samples allowed the correlation between thermal history and microstructure to be drawn.

This page intentionally left blank.

1 Background

The practice of using weld tempering passes is widespread in the ship building industry. Tempering passes are routinely incorporated within welding procedures to ensure that the underlying weld passes have the benefit of being re-heated and cooled. For the case of submarine pressure hull materials such HY-80 [1], the location, specification, and effectiveness of weld tempering passes has been the subject of a number of consulting requests and smaller investigations.

One tempering pass study examined the influence of weld heat input on the effectiveness of tempering [2]. This study revealed an anomalously high hardness within the coarse grained heat affected zone between two fill passes. Hardness profile measurements which ran through this region found that for both heat inputs of 600 and 900 J/mm the base metal in this region was significantly harder than the surrounding material (Figure 1). As the welding pass sequence is analogous to those experienced during weld build-up, concern was raised regarding the consequence of the weld thermal cycle on the base metal heat affected zone (HAZ).

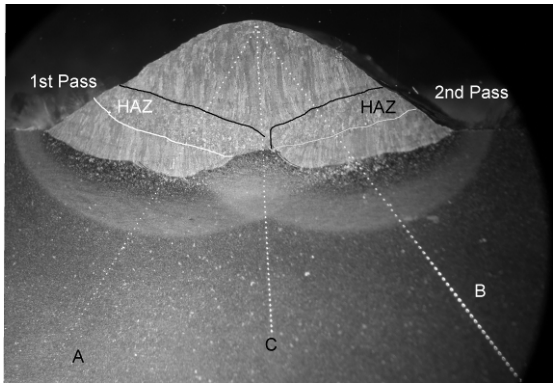

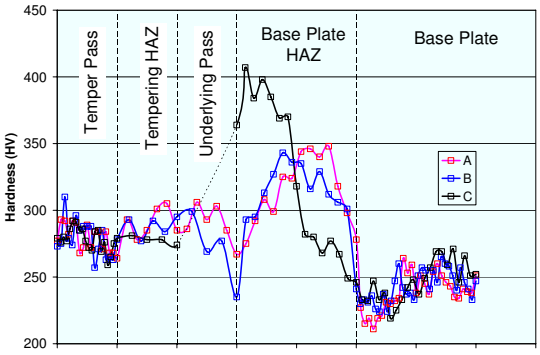

Figure 1 Previous study showing hardness traverse across weld boundaries. Each traverse starts at a common point in the temper pass and extends into the base plate.[2]

A subsequent investigation was therefore initiated in order to determine:

- Accurate thermal history of this hardened region,
- And to investigate the influence of heat input on the tempering of the underlying weld metal.

2 Welding Data Collection

This welding trial involved the deposition of weld metal on an instrumented plate in order to characterise the thermal cycle of the heat affected zone. The welding consisted of the deposition of at least three beads (passes) per block of weld. The layout of the blocks and passes is illustrated in Figure 2 in which the additional pass welded on block 1 is visible. Within each block (labelled lines 1 through 3), the starting and stop positions of each pass were staggered in order to ascertain the microstructural development which occurs during subsequent welding passes, with each block having a different specified heat input.

The target and actual welding conditions used for the three blocks are summarized in Tables 1 through 3. All of the welds were produced using the shielded manual arc welding process along with a 3.2 mm AWS A5.5 S9016G electrode while the base plate was HY-80. The welding procedure specified an initial minimum pre-heat of 120^{o}C with a maximum interpass temperatures of between 120-150^{o}C. All welds were produced in the flat (1G) position, with a 50% overlap for the first 2 passes followed by a tempering pass which extended from one weld to the other. All welding took place at Fleet Maintenance Facility Cape Breton on November 18, 2008. Drawings of the machined base plate and welding pass sequences are plotted in Figures 15 and 16 found in Annex A.

In order to characterize the heat affected zone thermal cycle, 24 gauge (510 μm diameter wire) glass braided K thermocouples were inserted into 7 holes drilled into the base metal along each weld line. The depths of the holes varied in an attempt to locate the end of the thermocouple within different regions of the HAZ. In nearly all cases the thermocouples were suitably positioned with a few being consumed within the fusion zone of the weld. Figure 3 illustrates a successfully positioned thermocouple which was located with the HAZ for all three passes. In all cases, the thermocouples were held in place with a high temperature thermo-setting epoxy [3] which is able to withstand temperatures of 540^{o}C when properly cured at 220ºC. During welding, the thermocouple data were logged at a frequency of 2 Hz using a National Instruments 9211 4 channel thermocouple unit. The seven pairs of thermocouples wires were twisted together and fed through a metal braided wire between the thermocouples and the data logger in order to minimize the influence of the surrounding electrical noise. Furthermore, the electrical return from the welding machine was isolated in order to reduce stray electrical currents which had previously been shown to given erroneous temperature spikes. The thermal outputs for each block of welds are plotted in Figures 17 through 19 in Annex B. From these plots, a measure of the weld travel speed was confirmed from the average time interval between peaks, which is included in the row labelled Travel Speed from Thermocouples in Tables 1 through 3.

Following welding, the plate was sectioned across the weld at each thermocouple location, which was used to determine the position of the thermocouple relative to the fusion boundary and visible heat affected zone. Unfortunately, not all of the cross sections left the thermocouples intact, and in these cases, the measurements were made from the deepest point of the drilled hole.

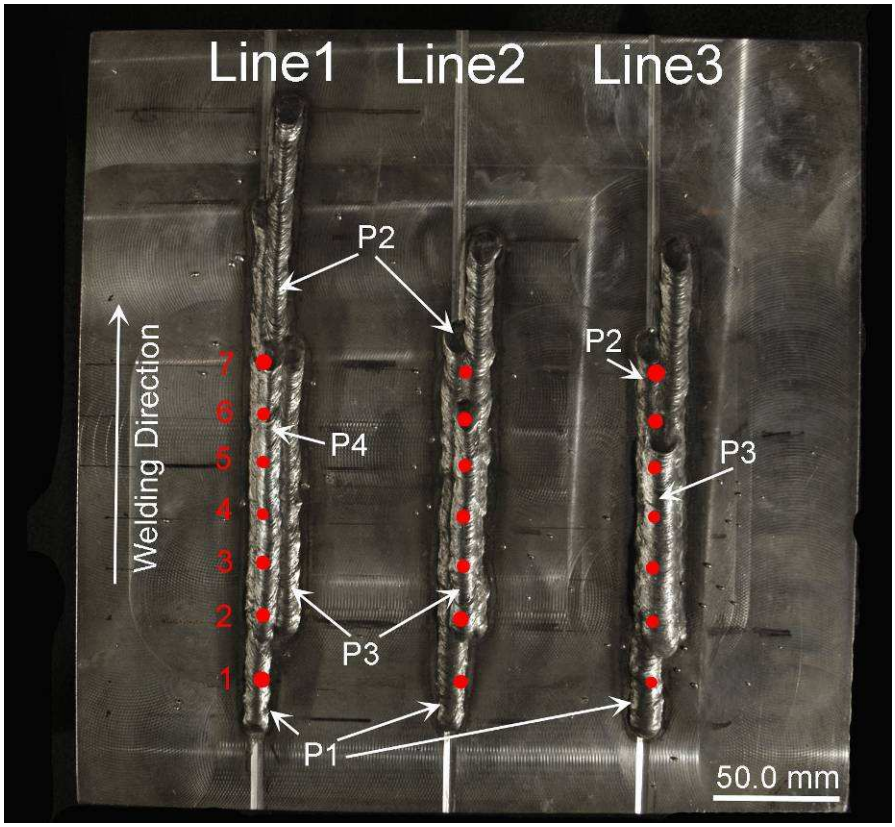

Figure 2 Completed bead on plate welds showing the location of passes and approximate locations of the blind hole thermocouples.

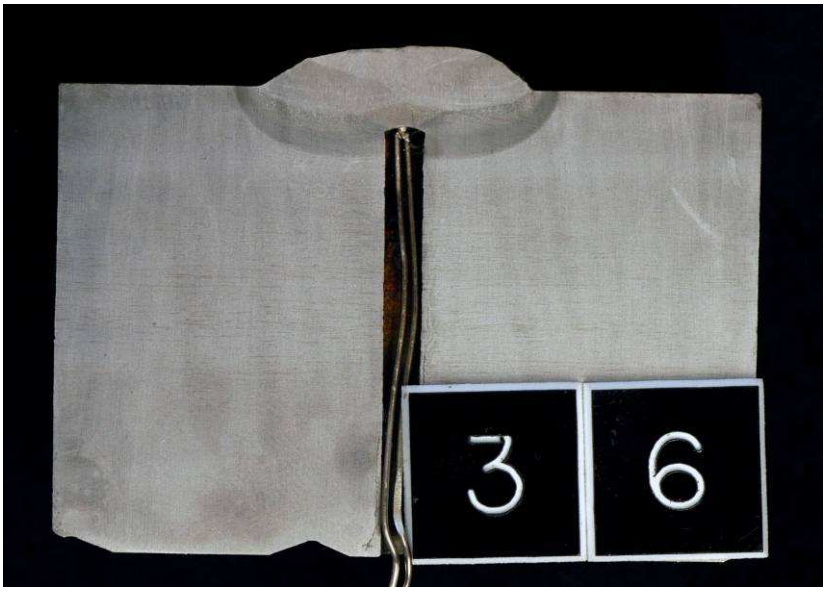

Figure 3 Blind hole thermocouple terminating within the HAZ of all three passes. (Line 3 TC 6)

Table 1 Welding Conditions – Line 1

	Pass1		Pass2		Pass3		Pass4	
	Target	Actual	Target	Actual	Target	Actual	Target	Actual
Current (Amp)	115.0	115.00	115.0	115.00	115.0	115.00		115.00
Voltage (V)	22.5	22.50	22.5	23.50	22.5	22.50		22.50
Pass Length (mm)	200.0	204.79	200.0	206.49	100.0	110.67		110.92
Time (s)	60.0	66.00	60.0	57.00	30.0	38.00		33.00
Travel Speed (mm/s)		3.10		3.62		2.91		3.36
Travel Speed from Thermocouples (mm/s)		3.16		3.12				4.68
Heat Input (J/mm)	776.25	833.91	776.25	745.99	776.25	888.42		769.83

Table 2 Welding Conditions – Line 2

	Pass1		Pass2		Pass3	
	Target	Actual	Target	Actual	Target	Actual
Current (Amp)	115.0	115.00	115.0	115.00	115.0	115.00
Voltage (V)	22.5	22.50	22.5	22.50	22.5	22.50
Pass Length (mm)	150.0	153.66	150.0	152.44	75.0	88.29
Time (s)	70.0	72.00	70.0	68.00	35.0	33.00
Travel Speed (mm/s)		2.13		2.24		2.68
Travel Speed from Thermocouples (mm/s)		2.45		2.42		2.74
Heat Input (J/mm)	1207.50	1212.43	1207.50	1154.23	1207.50	967.10

Table 3 Welding Conditions – Line 3

	Pass1		Pass2		Pass3	
	Target	Actual	Target	Actual	Target	Actual
Current (Amp)	115.0	115.00	115.0	115.00	115.0	115.00
Voltage (V)	22.5	22.50	22.5	22.50	22.5	22.50
Pass Length (mm)	150.0	152.20	150.0	158.54	75.0	88.05
Time (s)	80.0	78.00	80.0	78.00	40.0	53.00
Travel Speed (mm/s)	1.88	1.95	1.88	2.03	1.88	1.66
Travel Speed from Thermocouples (mm/s)		2.35		2.24		1.60
Heat Input (J/mm)	1380.00	1326.09	1380.00	1273.05	1380.00	1557.52

3 Results

3.1 Material Data

The chemical compositions of the base and as-deposited weld metal are summarized in Table 4. The chemical analysis of the base plate conforms to the HY-80 specification [1] while the as-deposited weld metal has a significantly leaner composition with significantly lower carbon, nickel, chromium and molybdenum than the base metal.

Table 4 Chemical Composition

	C	Si	P	Mn	Ni	Cr	Mo	S
Parent Material	0.14	0.15	0.006	0.27	2.2	1.1	0.25	0.002
As Deposited Weld Metal	0.08	0.17	0.009	1.3	1.1	0.23	0.18	0.002

For low carbon steels Poorhaydari [4] estimates the lower critical temperature (A_{C1}) and the melting temperature (T_m) in Celsius as:

$$A_{c1} = 723 - 30Ni - 25Mn - 5Co + 25Si + 30Al + 25Mo + 50V = 660$$
$$T_m = 1537 - 90C = 1524$$

Material lying between these two temperatures defines the visible heat affected zone.

3.2 Metallurgy

Optical micrographs of the as-deposited weldment, coarse grained heat affected zone and sub-critically reheated coarse grained heat affected zone are presented in Figures 4, 5 and 6, respectively. For all of the welding conditions, the as-deposited weld metal has the fine basket weave morphology of acicular ferrite which has desirable mechanical properties. The coarse grained heat affected zone which lies adjacent to the fusion boundary is comprised of fine lath martensite which transformed from relatively large austenitic grains. Lath, rather than plate martensite is typical of low carbon steels such as HY-80 [5, 6]. This martensitic structure is evident in all areas which have withstood peak temperatures above 1200ºC, in the so-called un-altered grain coarsened heat affected zone [7]. Regions which withstand secondary peak temperatures less than the A_{C1} temperature are considered to be within the sub critically reheated coarse grained heat affected zone. In this case, the secondary peak temperature is sufficient to temper the martensite. Notable differences in the optical micrographs of these two regions can be seen from Figures 5 and 6, which include the formation of a carbide rich phase on the prior austenite grain boundaries along with the recovery and recrystallization of the martensite [6].

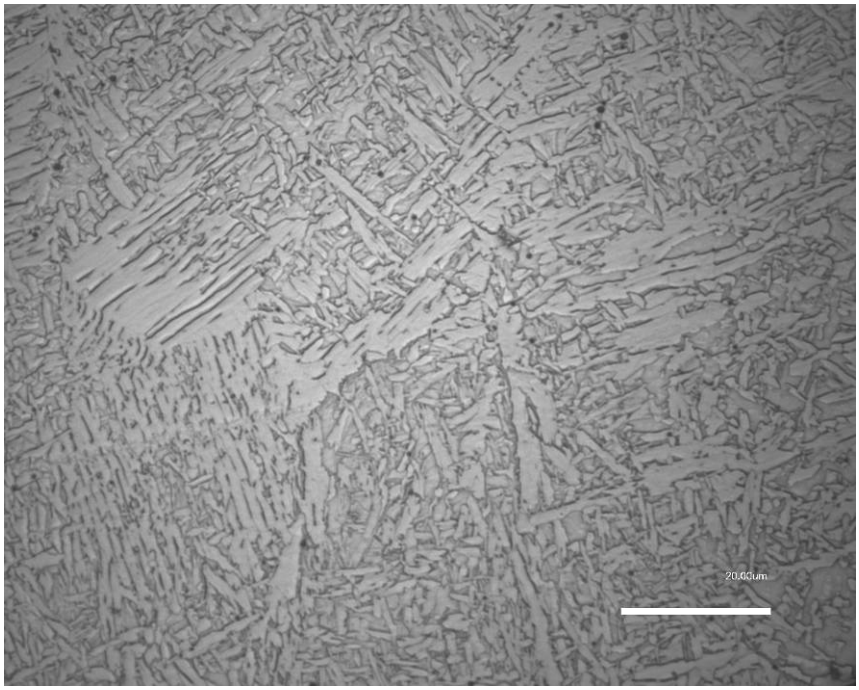

Figure 4 As-deposited weld metal consisting primarily of fine basket weave acicular ferrite. (Nital Etch, scale bar represents 20 μm).

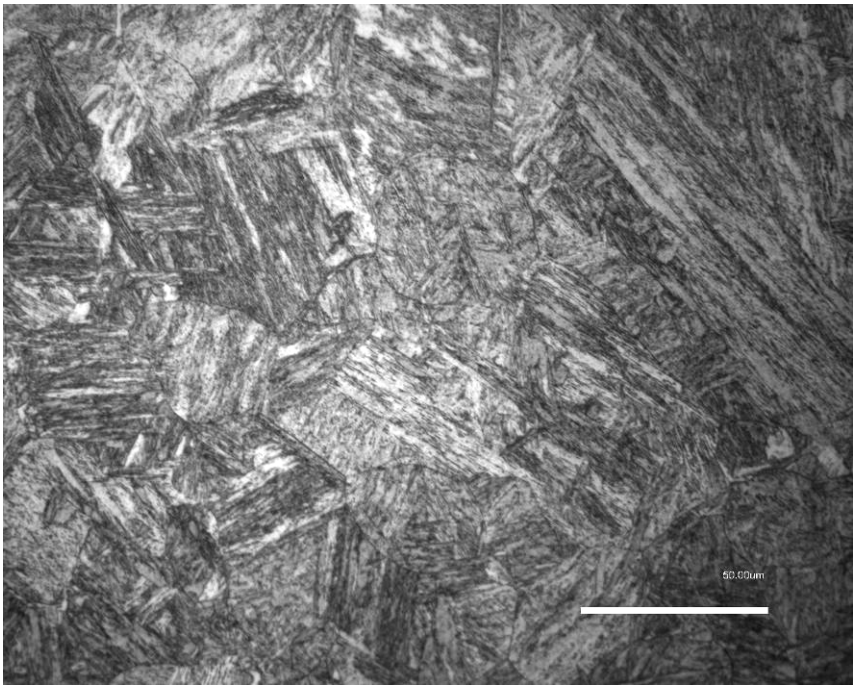

Figure 5 Untempered coarse grained heat affected zone close to the fusion line consisting of fine lath martensite with a hardness 450HV. (Nital Etch, scale bar represents 50 μm).

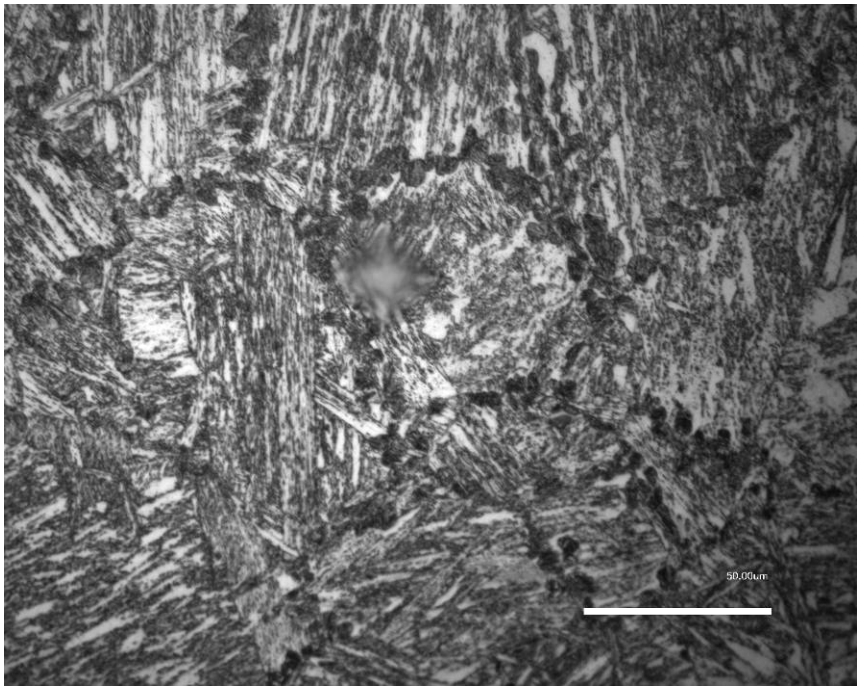

Figure 6 Subcritically reheated grain coarsened heat affected zone with a hardness of 300 HV (Nital Etch, Scale bar represents 50 μm).

3.3 Thermal Data

Knowledge of the welding thermal cycle is key to understanding the metallographic changes in the fusion and heat affected zones. While a single analytical description of both the heating and cooling cycles remains elusive, the key variables including the peak temperature and cooling rate are readily determined from the steady state conduction equations [8]. Adams [9] developed simplified engineering thermal conduction expressions which have the advantage of providing the peak temperatures relative the fusion zone. However, these analytical expressions consider the temperature profile along the centerline of the weld with 3D and 2D solutions corresponding to whether or not the back face of the plate contributes as a thermal boundary condition. The transition between these two bounding solutions is determined by the relative plate thickness: $d\sqrt{\frac{\rho C_p (T_c - T_o}{q/V}}$ where the variables are identified in Table 6. Relative plate thicknesses greater than 0.75 are considered to be thick, while relative plate thicknesses less than 0.75 are considered to follow the thin plate solution. For the present weld plate geometry, the thermal boundary conditions at the deepest point of the weld would correspond with the 3D solutions; however towards the edges of the weld, the thermal boundary conditions approach 2D.

Table 5 Analytical Heat Flow Expression for 3D and 2D plates

	3D - Thick Plate	2D – Thin Plate
Peak Temp (C) [4]	$T_p - T_0 = \left(\frac{2}{\pi e}\right)\frac{q/V}{\rho C_p r^2}$	$T_p - T_0 = \sqrt{\frac{2}{\pi e}}\frac{q/V}{d\rho C_p 2r}$
Cooling Rate (C/s) [9]	$\frac{dT}{dX}V = 2\pi K\frac{V}{q}\left(T_c - T_o\right)^2$	$\frac{dT}{dX}V = 2\pi K\rho C_p\left(\frac{dV}{q}\right)^2\left(T_c - T_0\right)^3$

As seen in Table 5, the peak temperature is related to net the heat input *q/V* and the distance *r* away from the fusion zone, while the cooling rate is largely independent of its location within the HAZ. Figure 7 is a plot of the peak temperature profile within the HAZ for both the 2D and 3D solutions. From these solutions, the width of the HAZ can be estimated for a fixed set of welding conditions.

Table 6 Thermal Coefficients

ρC_p	Volumetric Specific Heat	0.0044	J/mm^3 C
K	Thermal Conductivity	0.05	J/(mm s C)
α	Thermal Diffusivity = $K/\rho C_p$	11.36	mm^2 / s
r	Radial distance from edge of fusion zone	0-4	mm
T_p	Peak Temperature	To Be Determined	C
T_c	Specified Cooling Temp	From 800 to 500	C
T_m	Melting Temperature	1524	C
A_{C1}	Lower Critical Temperature on heating	653.85	C
T_o	Interpass Temperature	From Thermal Data	C
η	Thermal Efficiency	0.7	Unitless
q	Arc Power $q = \eta EI$	From Tabulated Data	J/s
V	Travel Speed	From Tabulated Data	mm/s
d	Thickness of Base Plate	32	(mm)

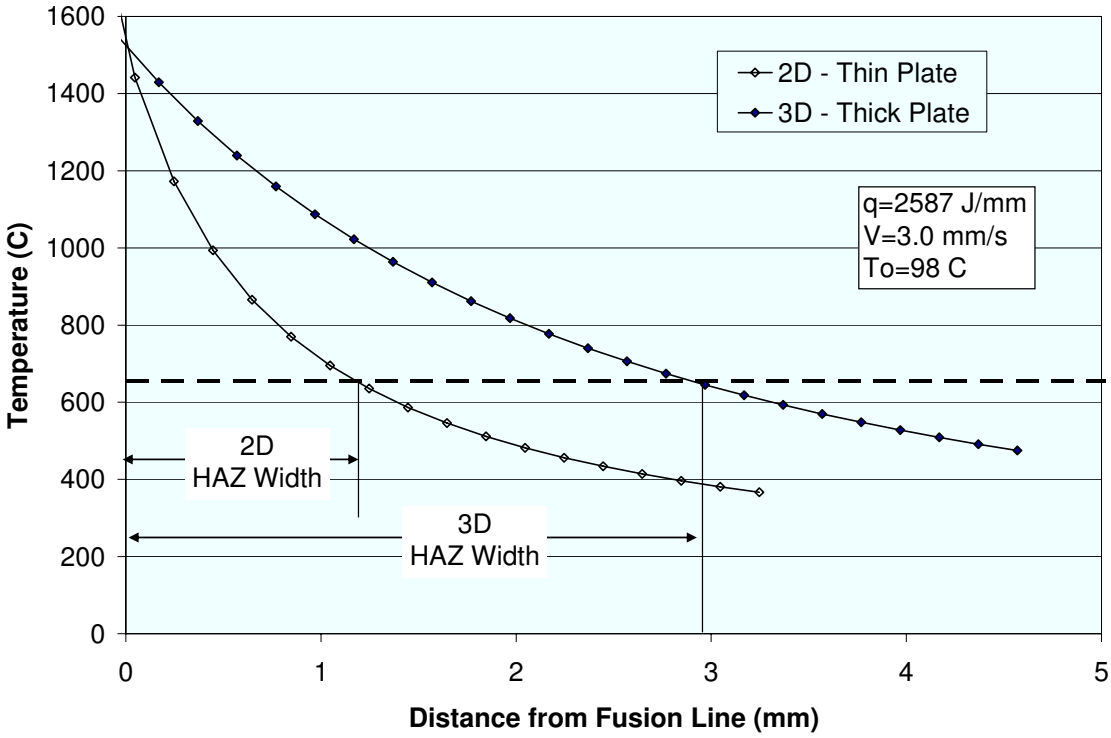

Figure 7 Analytical peak temperature distributions for 2D and 3D boundary conditions.

Peak temperatures for all of the thermocouples as a function of distance from the fusion line are plotted in Figure 8 along with the 2D analytical temperature solutions found in Table 5. The 2D rather than the 3D solutions are used since they better represent the thermal boundary conditions for the location of each thermocouple with the HAZ. The three circled "outliers" correspond to the thermocouples which were fused by a previous welding pass, and hence altered the predictable thermo-electrical properties at the junction. Experimentally, the trend of an increasing temperature gradient with increasing heat input is correctly predicted.

Similarly, the average cooling rates between 800-500ºC are plotted in Figure *9* with matching 2D analytical expressions from Table 5. As predicted by these analytical expressions, the cooling rates within the HAZ appear relatively independent of the thermocouple location.

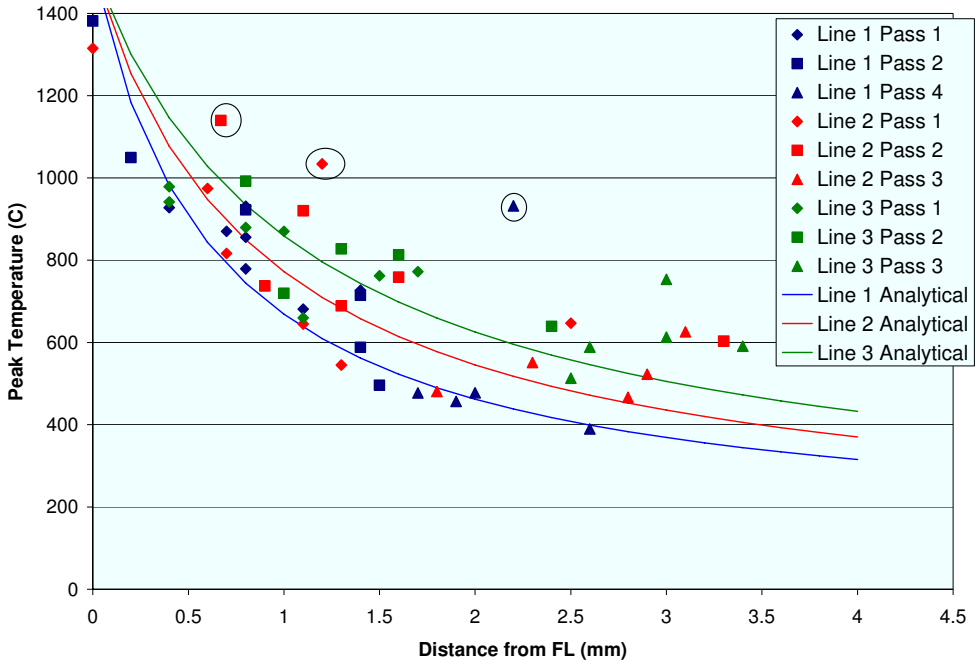

Figure 8 Experimental and predicted analytical peak temperature. Circled data points coincide with fused thermocouples.

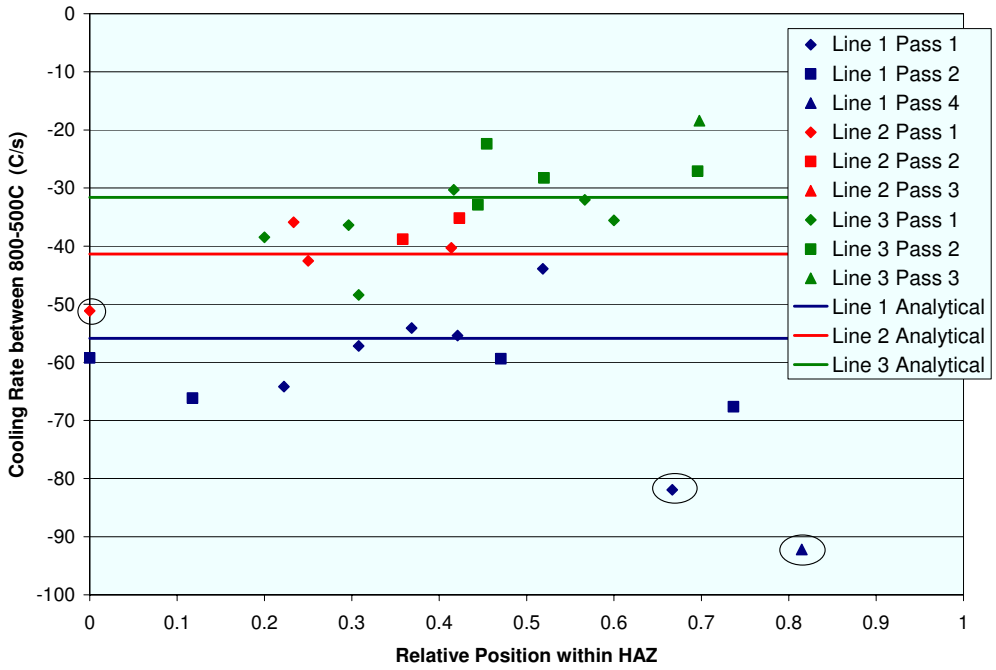

Figure 9 Cooling between 800-500ºC rates within HAZ. Circled points correspond with fused thermocouples.

3.4 Hardness Data

Hardness plots were acquired from transverse sections along each of the three weld lines. A rectangular array of microhardness indents was made at 500 μm intervals in each of these transverse slices in order to map the entire surface. Figure 10 is the polished and etched section corresponding to transverse section 3D shown in Figure 20 of Annex C, and the associated microhardness map. Klemm Colour etching of the weld [10] clearly differentiates the three welding passes (fusion boundary highlighted in red) along with their heat affected zones (outlined in white). For clarity, the weld and visible heat affected zone boundaries are highlighted in both the macro-photograph and the hardness plot. In doing so a number of features become clear:

1. Weld hardness appears to be uniform for all three weld passes.

2. The HAZ hardness is dependent on the distance from the visible heat affected zone boundary.

3. The most effective tempering occurs beyond the visible heat affected zone boundary.

These observations follow not only from Figure 10, but from all of the microhardness maps illustrated in Figures 21-29. From detailed inspection of these figures, the development of the weld tempering process can be better understood. Figures 21, 24 and 27 reveal that after a single bead on plate the hardness of the material within the coarse grained heat affected zone has a range in hardness between 400-430 HV. This material withstood peak temperatures above the A_{C3} meaning that all of the ferrite is expected to transform to austenite. For the material which is intecritically re-heated between the A_{C3} and A_{C1} temperatures, the hardness has an intermediate hardness between the unaffected base plate and the harder coarse grained HAZ. These trends in hardness appear to be independent of the limited range of weld heat inputs and correspond with a similar study examining the hardness of the fusion zone in autogeneous laser beam welds [11]. The similarity of these measurements suggests that a hardness in the range of 400-430 HV is representative of the untempered martensite which develops over a wide range of cooling rates [12].

The influence of subsequent weld passes on the hardness is shown in Figures 22, 25 and 28 in Annex C. By superimposing the contours of the fusion boundary and the extent of the visible HAZ onto the hardness maps, the location of the tempered region can be identified. This tempered region lies beyond the visible HAZ boundary and extends into the subcritical heat affected zone of the current pass, which is associated with peak temperatures less than A_{C1} [7, 13]. Interestingly, the hardness of the weld metal was unaffected by the second and all subsequent welding passes.

The final overlapping layer further develops the aforementioned tempering process. Material which experience temperatures less than A_{C1} are tempered, while material which experiences peak temperatures between the A_{C1} and T_M are only partially tempered. Thus the spatial distribution of the peak temperature profile is seen to govern tempering.

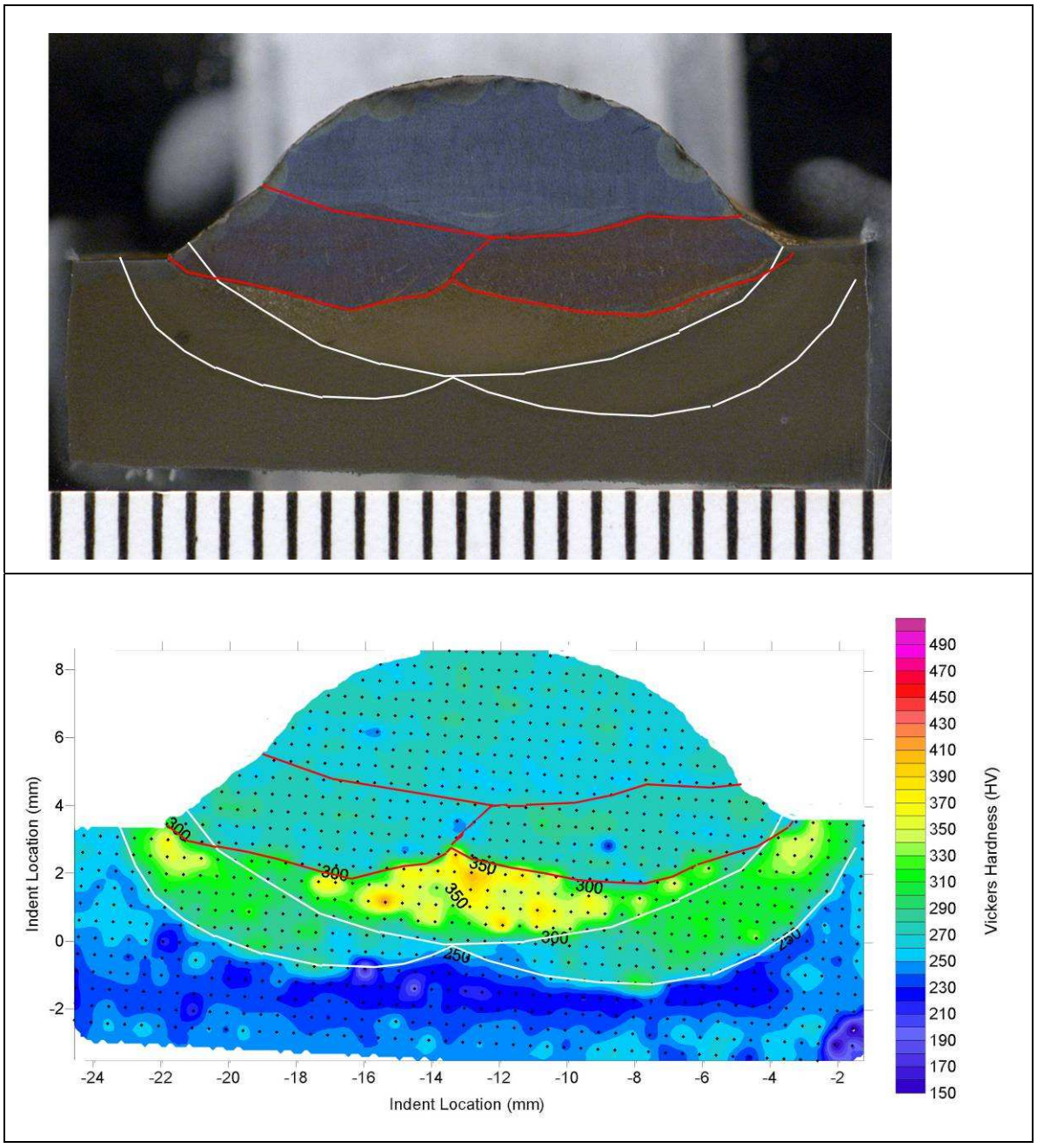

Figure 10 Colour macro etched sample and Microhardness Vickers Map. Contour lines of the fusion boundary and the extent of the visible HAZ have been added for clarity.

4 Discussion

Based on available Continuous Cooling Transformation (CCT) data for HY-80 [12, 14, 15], martensite would be expected in the heat affected zones for all but the slowest cooling rates associated with welding. For this reason, the microstructures within the heat affected zones for all of the welding conditions appear to be similar, with only the width of the HAZ determined by the peak temperature distribution.

The decrease in hardness during weld tempering is brought about primarily through the annihilation of dislocations and formation of fine precipitates [7, 16]. In order for tempering to occur, the peak temperature must be below the A_{C1} temperature which suppresses the martensite formation during cooling. Thus, optimum tempering is found to occur in the so-called subcritically reheated zone. As illustrated in Figures 5 and 6, a significant microstructural transformation occurs during this subcritical reheating. This includes the formation of a carbide rich phase along the prior austenite grain boundaries, along with the recovery and recrystallization of the martensitic laths. The recrystallization and recovery process involves the annihilation of the dislocation substructure resulting in a dislocation-free ferritic phase [6].

The effectiveness of the tempering process is examined in detail in Figures 11 and 12. In these figures, hardness measurements along two lines are extracted from the data set and replotted as the distance from the visible HAZ, which is outlined in white. Hardness data from the points along the lines identified as Tempered and Partially Tempered in Figure 11 are plotted in Figure 12 both before and after the final tempering pass along with the predicted peak temperature distribution. The predicted peak temperature distribution for the tempering pass follows the thermal calibration data which was developed in Section 3.3, with the visible HAZ boundary coinciding with the A_{C1} temperature. The effectiveness that the subsequent welding pass has on reducing the hardness of the coarse grained heat affected zone of the primary pass is clearly demonstrated by comparing the discrete green points with the green line. Furthermore, the assertion that optimal tempering is associated with subcritical reheating is demonstrated by the sudden decrease in the hardness beyond the visible HAZ boundary.

While the tempered heat affected zone will be harder than the surrounding base or weld metal, this is neither unique nor new. In 1991 Sumpter indicated that the HAZ of Q1N is typically in the region of 400 HV [17]. This was confirmed by recent microhardness maps from a circumferential weld seam extracted from HMCS VICTORIA shown in Figure 13. In this figure, a microhardness map is superimposed on a macro photograph which has been colour-etched to reveal the pass sequences. Apart from the area corresponding with the last pass on the bottom right corner, the hardness measurements are less than 380 HV while adjacent to the last pass, the hardness is greater than 400 HV. This corresponds to the untempered regions found in the current study. While one would expect such a high hardness to be associated with brittle fracture, Sumpter suggests that the high hardness effectively shields the HAZ and deflects crack front into either weld or base metal which is significantly softer [17], but this argument is only valid for running and not initiating cracks. The fact that the untempered martensite in the coarse-grained heat affected zone is brittle was clearly witnessed by numerous cracks around the Vickers Hardness indents as shown in Figure 14.

The recognition that the optimum tempering occurs at peak temperatures less than A_{C1} is important in the design of weld tempering sequences. For the current combination of HY-80 base plate and AWS 9016G welding consumable, it is the HY-80 base plate rather than the weld metal which requires tempering. Therefore, welding procedures need to account for the peak temperature profiles to insure that the A_{C1} temperature falls within the coarse grained heat affected zone of the underlying base plate.

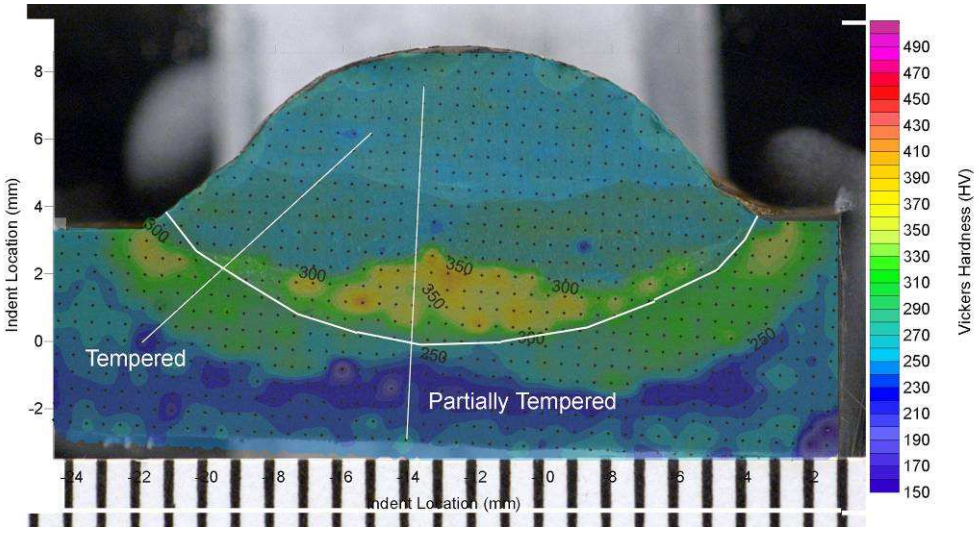

Figure 11 Location of tempered and partially tempered line profiles plotted in Figure 12

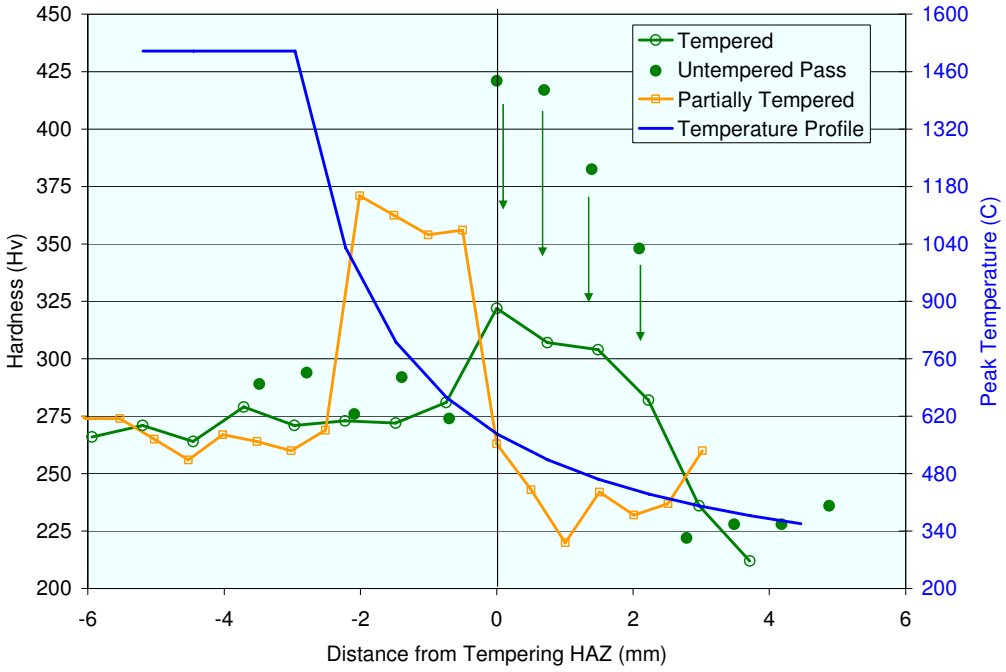

Figure 12 Tempering effectiveness. Location of the tempering line profiles are shown in Figure 11. (Line 3)

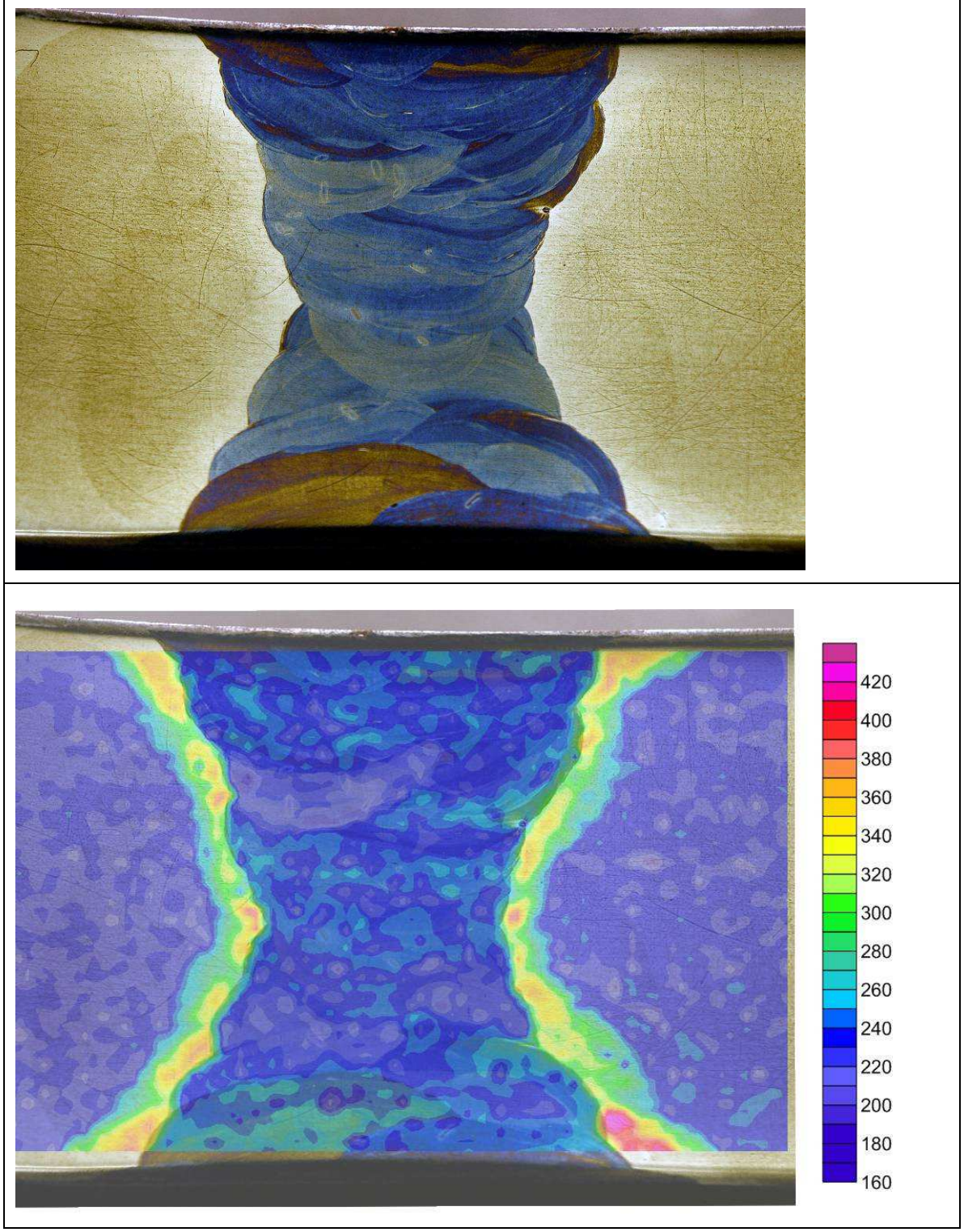

Figure 13 Overlaid microhardness plot obtained from a circumferential butt weld on HMCS VICTORIA.

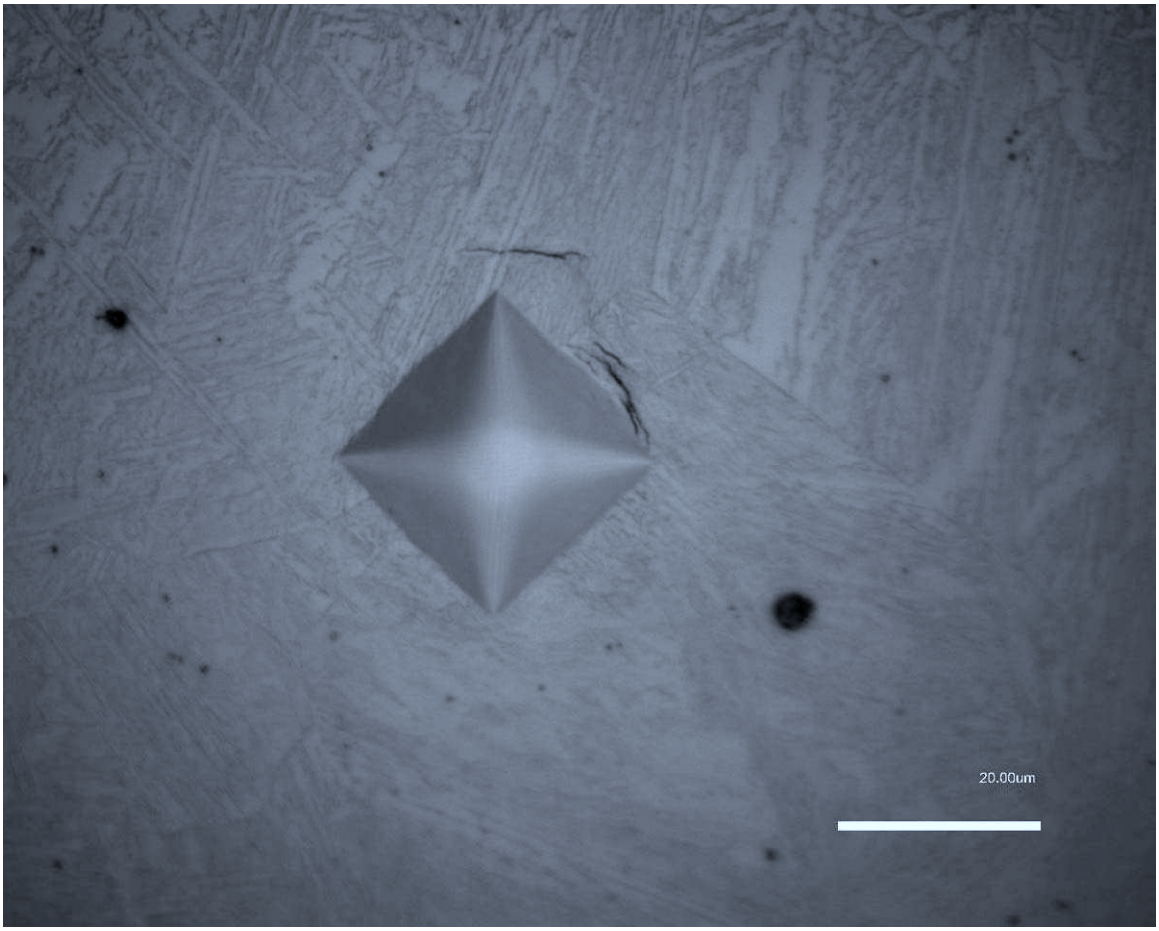

Figure 14 Crack emanating from a micro hardness indent in the untempered coarse grained heat affected zone. (Nital etch, scale bar represents 20 μm).

5 Conclusion

This study was motivated in an attempt to understand the anomalous tempering behaviour in a previous bead on plate welding study [2]. The anomaly in the previous study was that the tempering pass did not appear to anneal the base plate, but rather generated a harder microstructure. The results of this report explain this anomalous behaviour and reveal the following:

1. The coarse grained heat affected zone is comprised of a hard and brittle martensitic phase.

2. Reheating this martensitic phase below the lower critical temperature (A_{C1}) allows for the recrystallization and recovery of the martensitic structure, diffusion and precipitation of carbide rich phase.

3. Re-heating above the upper-critical temperature (A_{C3}) leads to limited tempering as the austenite to martensite transformation occurs upon cooling.

4. The location of peak tempering is adjacent to the visible heat affected zone.

5. For HY-80 steels and AWS 9016G consumables, weld tempering sequences need to be designed to focus on reheating the coarse grained heat affected zone of the base plate rather than the weld metal.

With this knowledge, the previous anomalous behaviour is explained.

References

[1] MIL-S-16216K(SH) Steel Plate, Alloy, Structural, High Yield Strength (HY-80 and HY-100), USA, 1987.

[2] Bayley, C.J., *Influence of Weld Heat Input on the Effectiveness of Tempering – HMCS Victoria*, DRDC Atlantic/DLP/3715-1G-06, May 2008.

[3] *Hi-Temp Lab-Metal*, Alvin products.

[4] Poorhaydari, K., Patchett, B.M., and Ivey, D.G., *Estimation of Cooling Rate in the Welding of Plates with Intermediate Thickness.* Welding Journal, 2005. **84**(10): p. 149-155.

[5] Krauss, G., *Principles of Heat Treatment of Steel*. 1980, Metals Park: ASM.

[6] Speich, G.R. and Taylor, K.A., *Tempering of Ferrous Martensites*, in *Martensite, a Tribute to Morris Cohen*, Olson, G.B. and Owen, W.S., Editors. 1992, ASM: Materials Park.

[7] Vishnu, P.R., *Solid-State Transformations in Weldments*, in *Volume 6 Welding, Brazing and Soldering*, LeRoy Olson, D., et al., Editors. 2007, ASM: Materials Park.

[8] Tsai, C.L. and Tso, C.M., *Heat Flow in Fusion Welding*, in *Welding, Brazing and Soldering*. 2007, ASM.

[9] Adams, C.M., *Cooling Rates and Peak Temperatures in Fusion Welding.* Welding Journal, 1958. **5**: p. 210s-215s.

[10] Vander Voort, G.F., *Color Metallography*, in *ASM Handbook Volume 9: Metallography and Microstructure*, Vander Voort, G.F., Editor. 2004, ASM: Materials Park.

[11] Bayley, C.J. and Cao, X., *Fibre Laser Welding of HY-80 Steel: Procedure Development and Testing*, DRDC Atlantic, TM 2009-187, 2009.

[12] ASM, *Atlas of Time-Temperature Diagrams for Irons and Steels*. 1991, ASM. p. 566.

[13] Gianetto, J.A., et al., *Heat-Affected Zone Toughness of a TMCP Steel Designed for Low-Temperature Applications.* Journal of Offshore Mechanics and Arctic Engineering, 1997. **119**: p. 11.

[14] *HY-80*, in *Alloy Digest Data on World Wide Metals and Alloys*. 2002, Engineering Alloys Digest: Upper Montclair, NJ.

[15] Haidemenopoulos, G.N., *Heat Flow and Material Degradation During Laser Metal Forming*, in *Ocean Engineering*. 1985, MIT: Boston. p. 144.

[16] Porter, D.A. and Easterling, K.E., *Phase Transformations in Metals an Alloys*. 1991: Chapman and Hall.

[17] Sumpter, J.D.G. *Fracture Avoidance in Submarine and Ships*. In *Advances in Marine Structures*. 1991. Dumfermline, Scotland.

This page intentionally left blank.

Annex A Machine Instructions

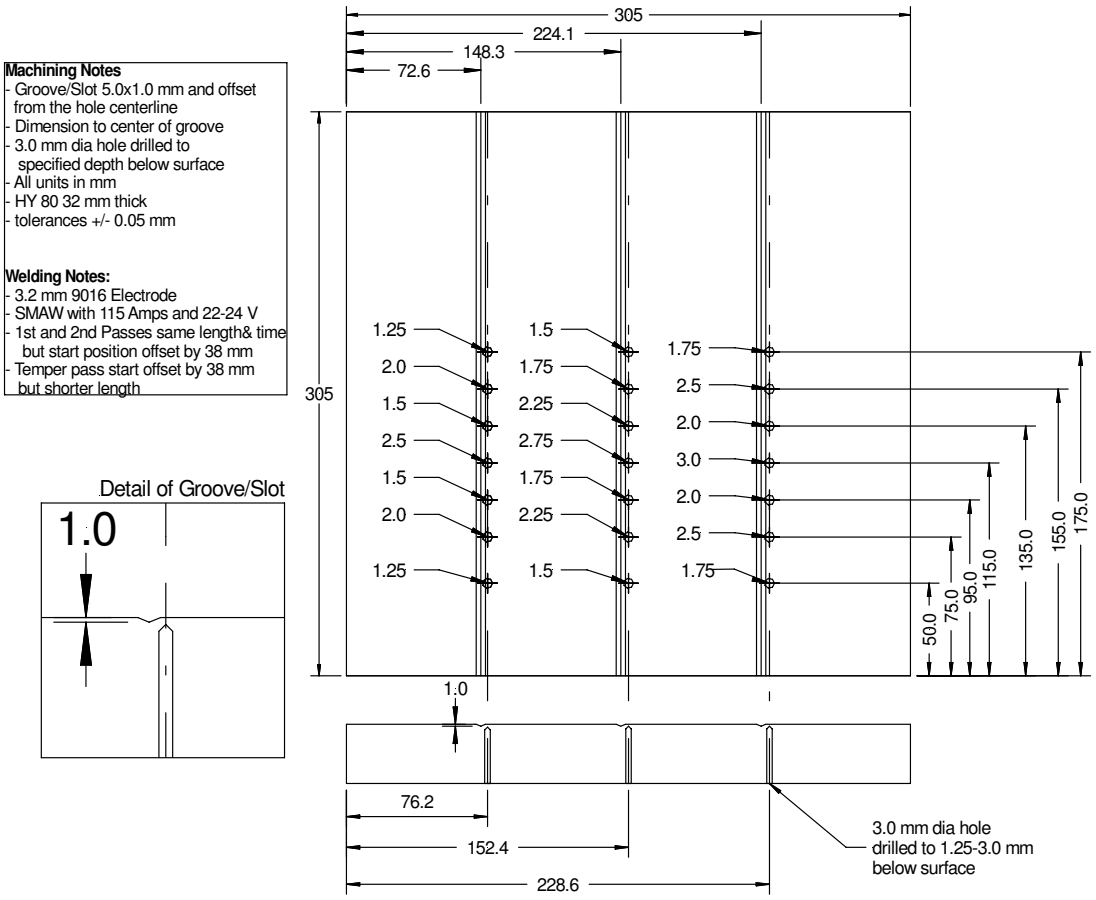

Figure 15 Blind hole thermocouple locations

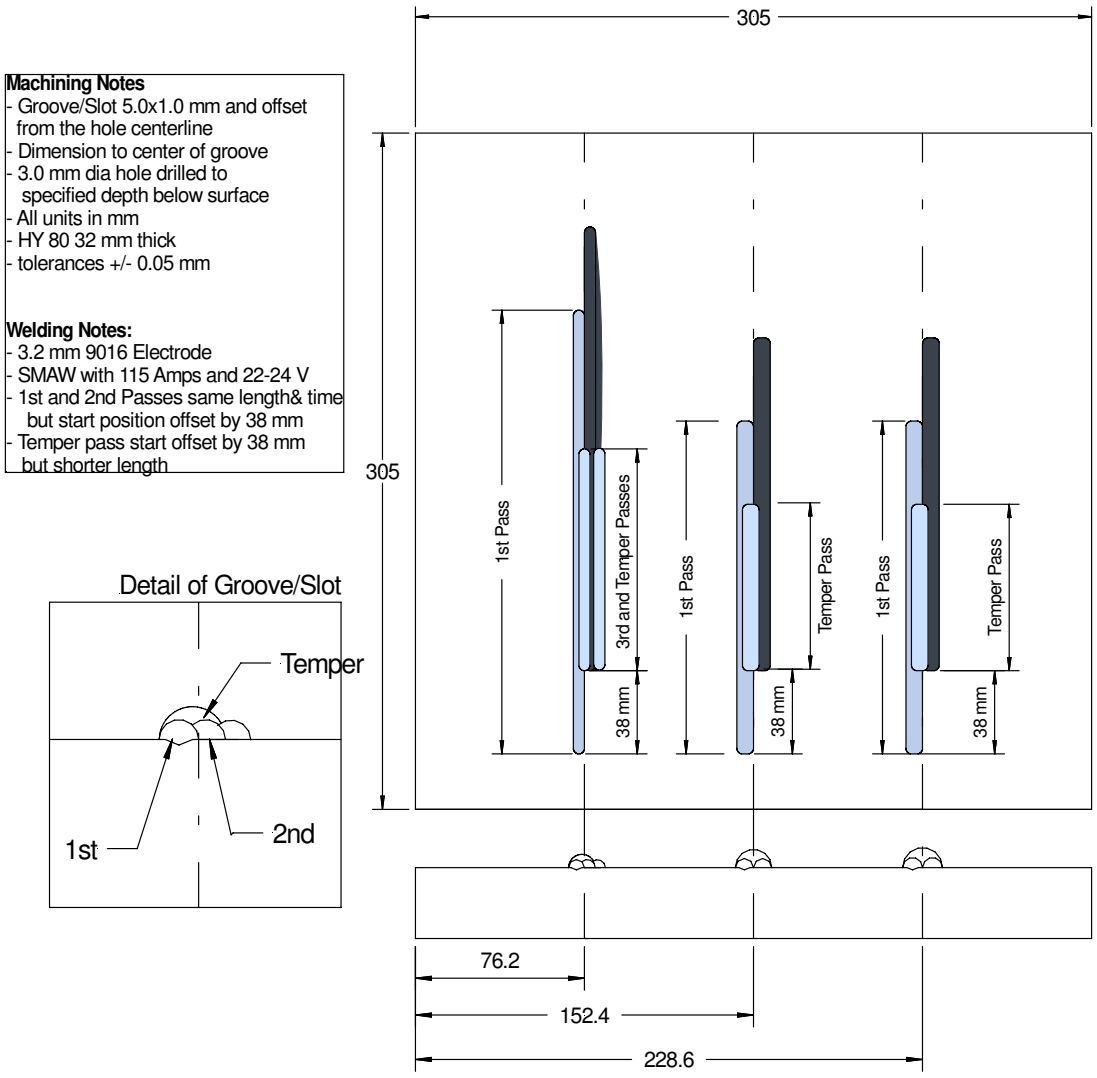

Figure 16 Welding Plan.

Annex B Thermal Data

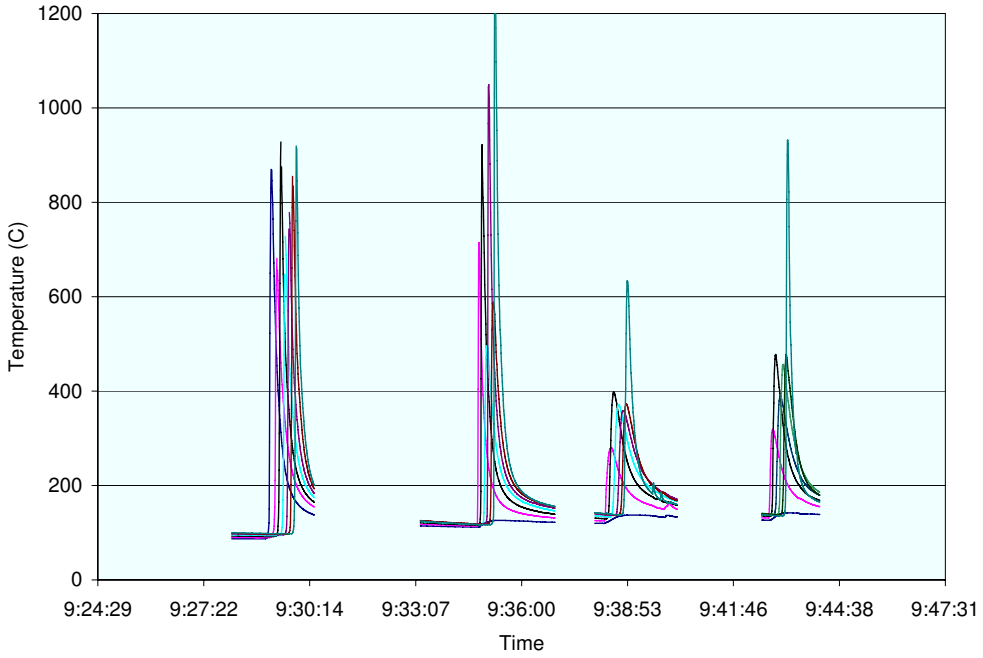

Figure 17 Line 1 thermal histories

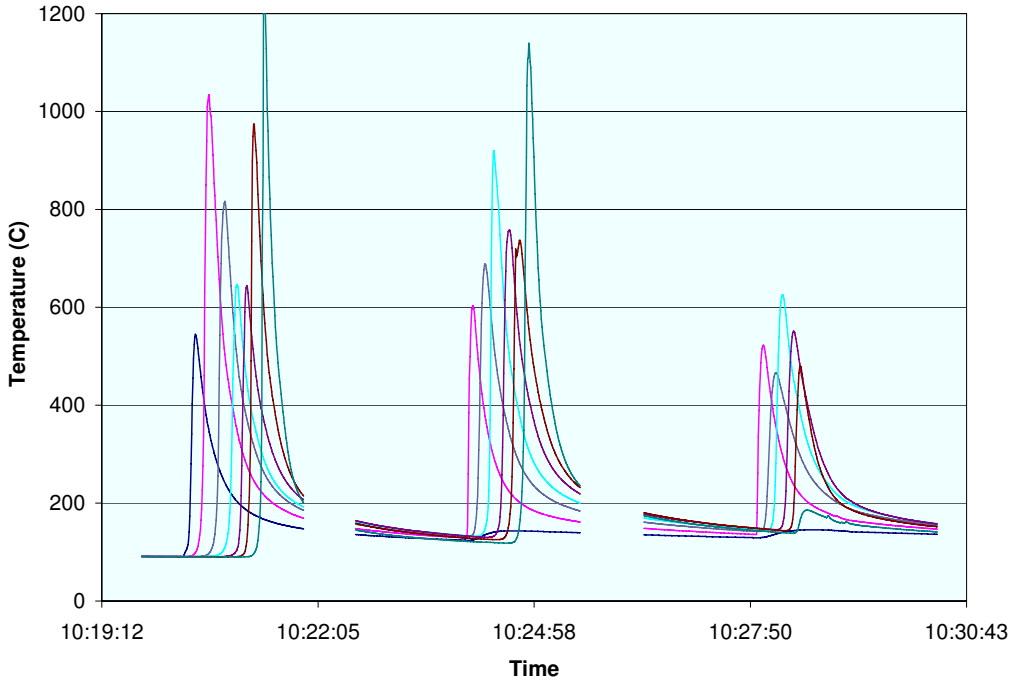

Figure 18 Line 2 thermal histories

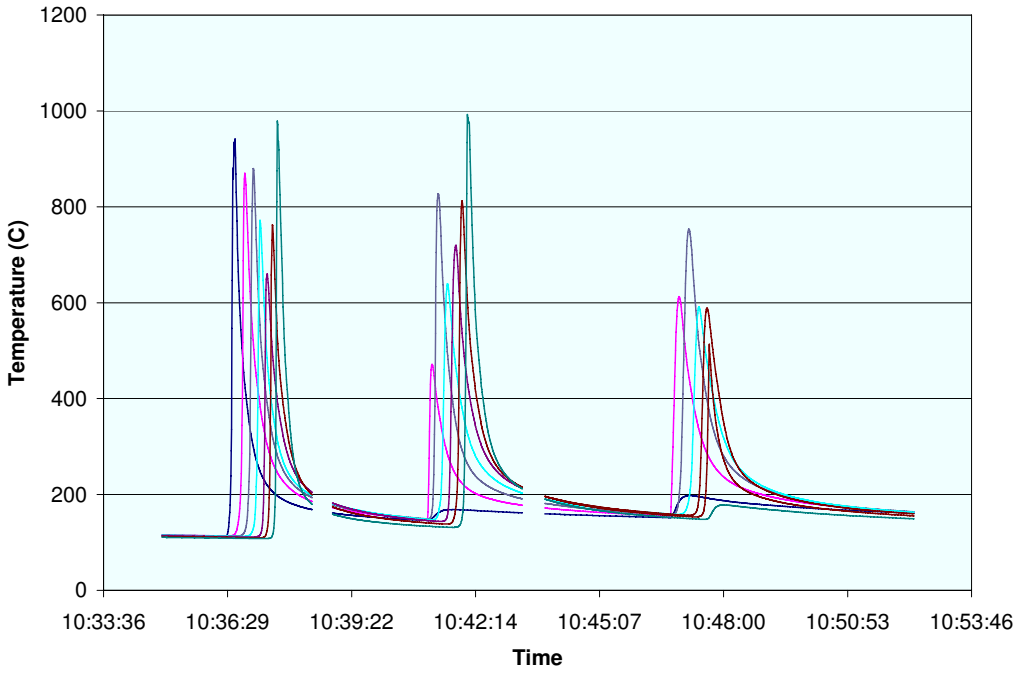

Figure 19 Line 3 thermal histories

Annex C Microhardness Plots

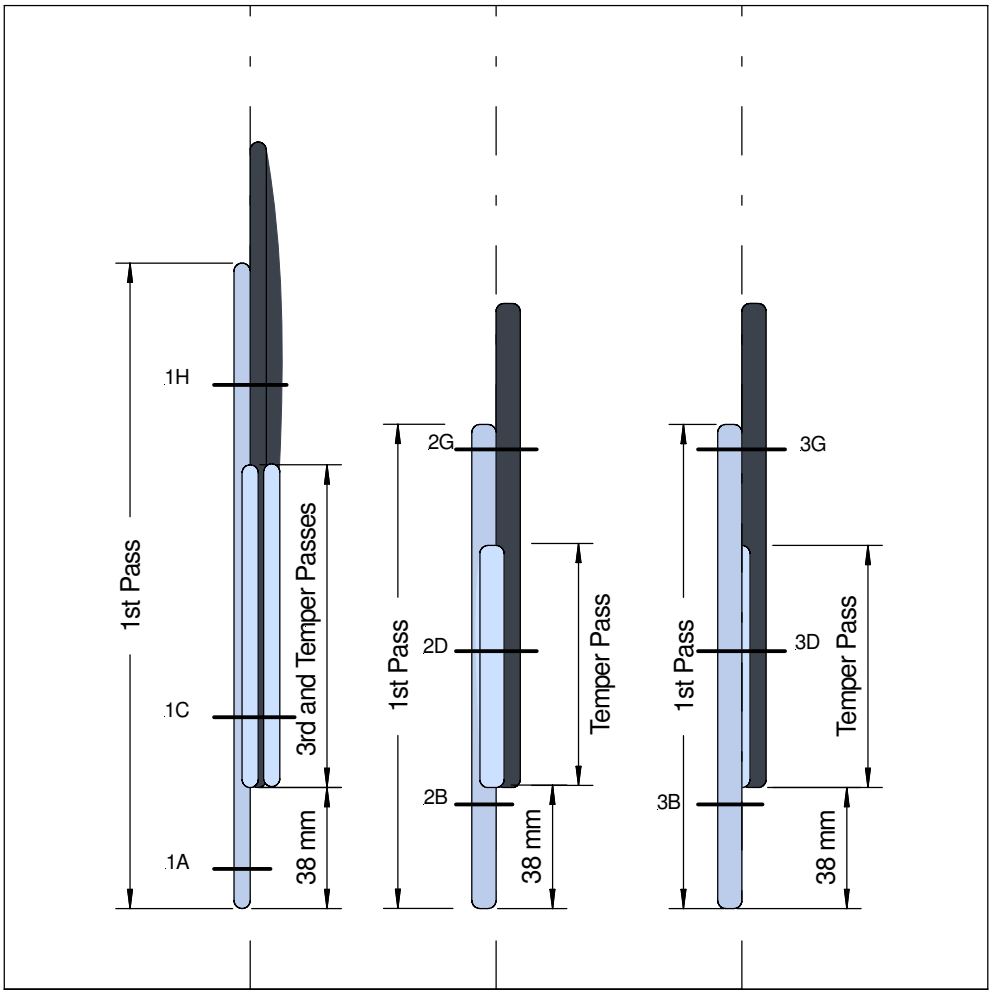

Figure 20 Location of microhardness cross sections

C.1 Line 1

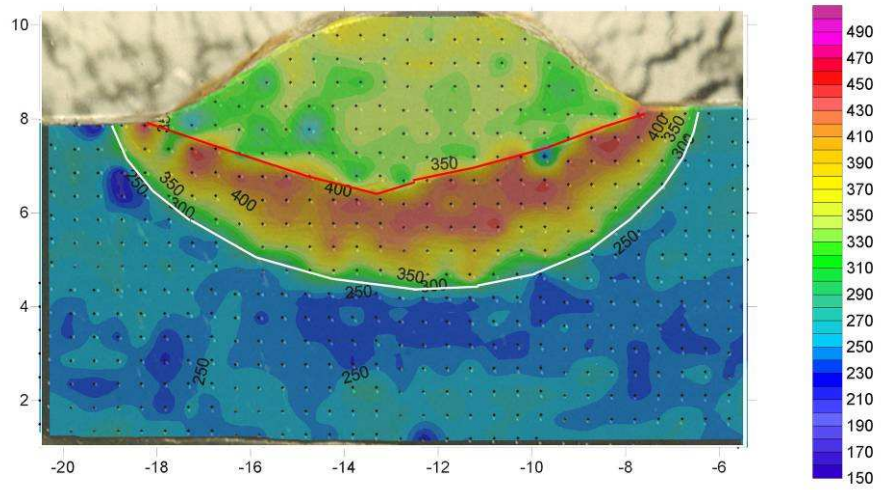

Figure 21 Location 1A (Single Pass)

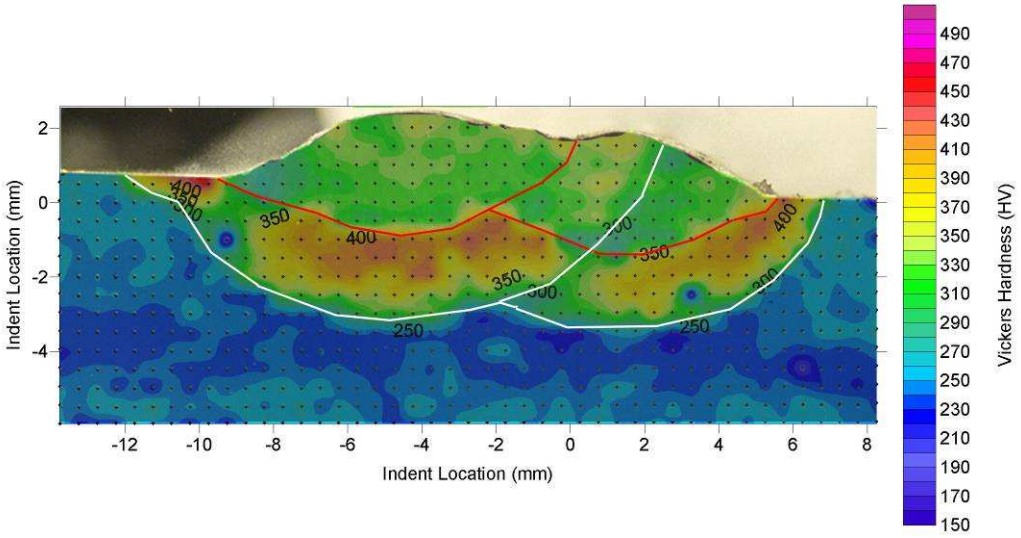

Figure 22 Location 1H (Two passes side by side)

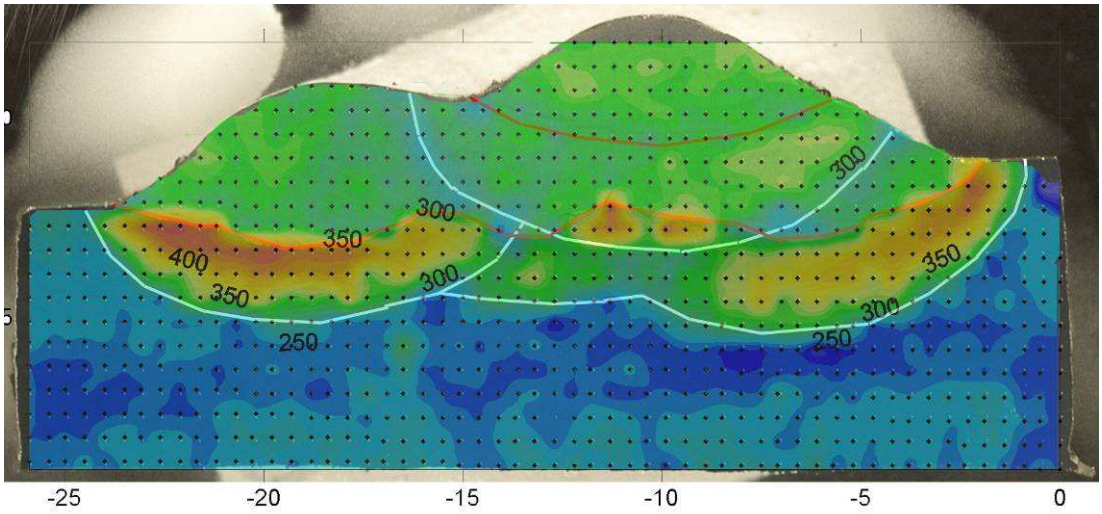

Figure 23 Location 1C (Four passes – Three side by side plus one temper pass)

C.2 Line 2

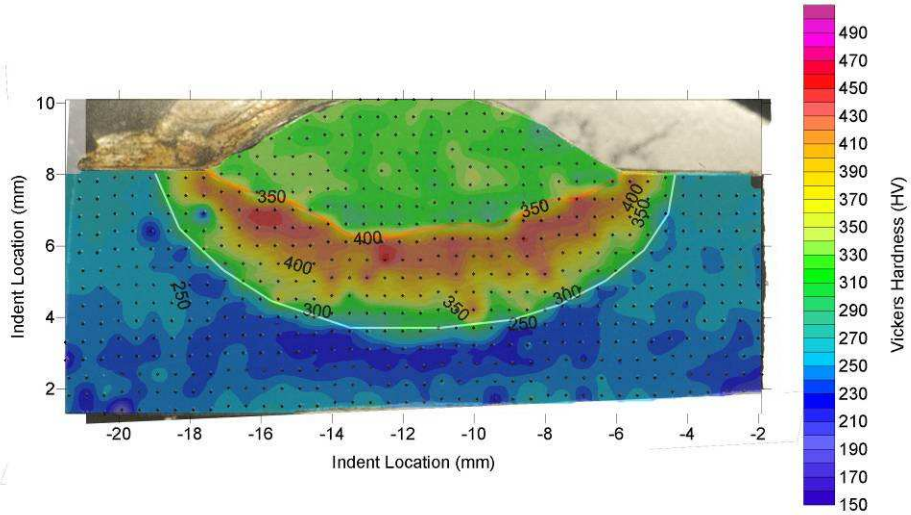

Figure 24 Location 2B (Single pass)

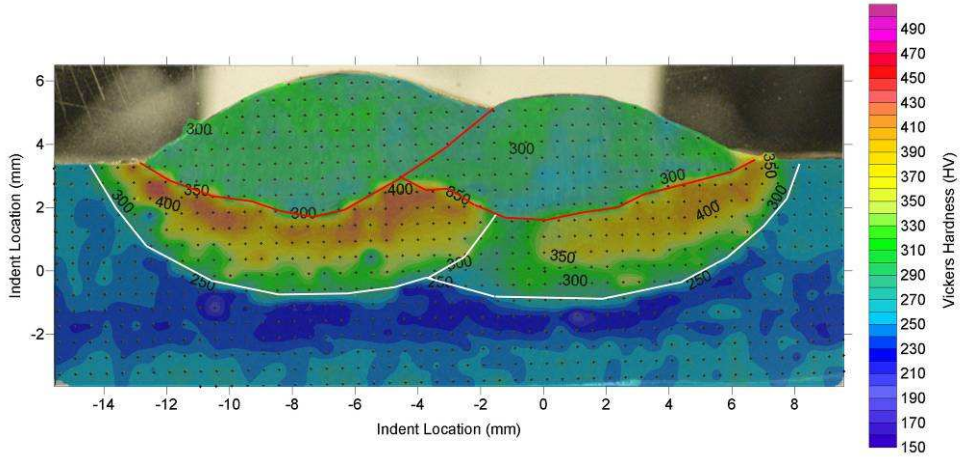

Figure 25 Location 2G (Two passes side by side)

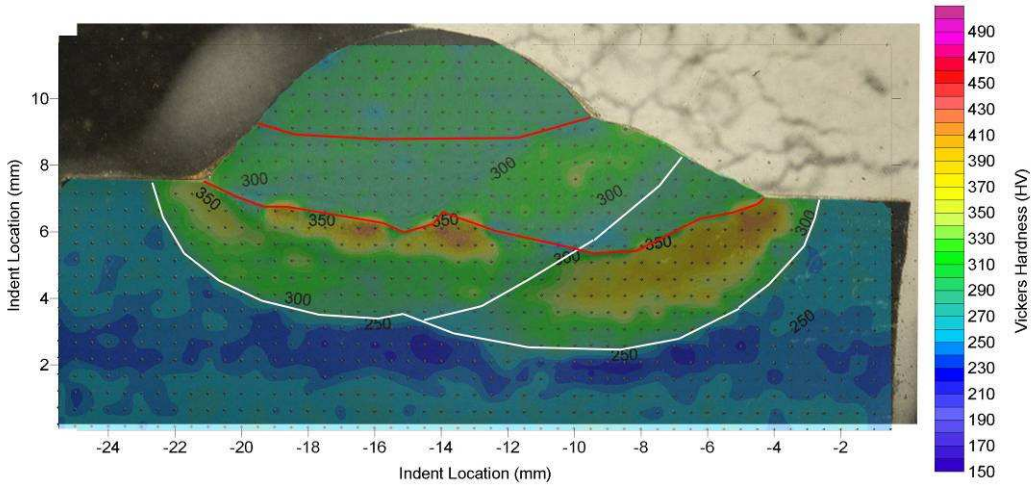

Figure 26 Location 2D (Three passes including temper pass)

C.3 Line 3

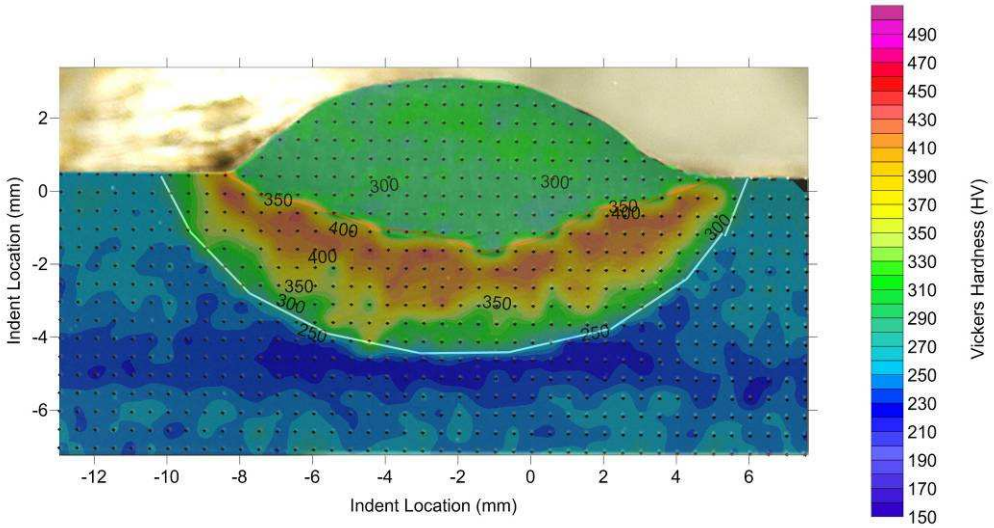

Figure 27 3B (Single pass)

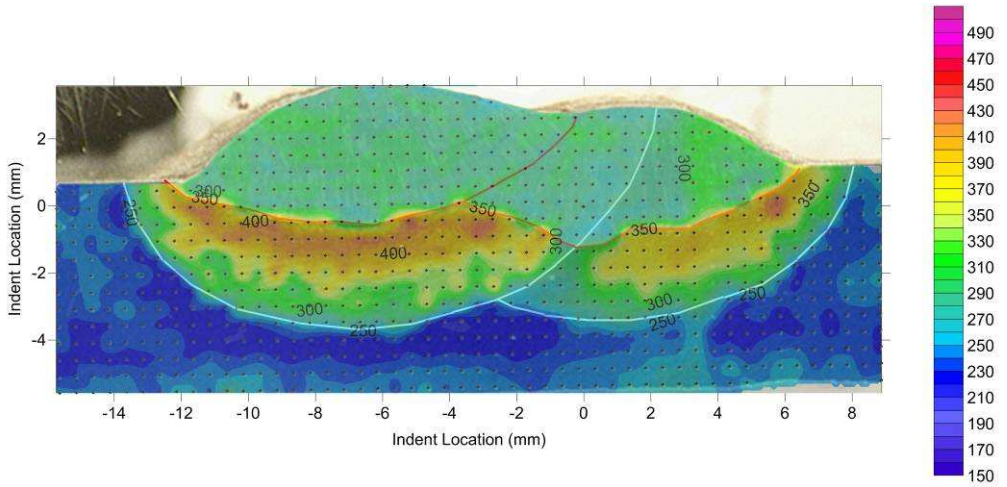

Figure 28 3G (Two passes side by side)

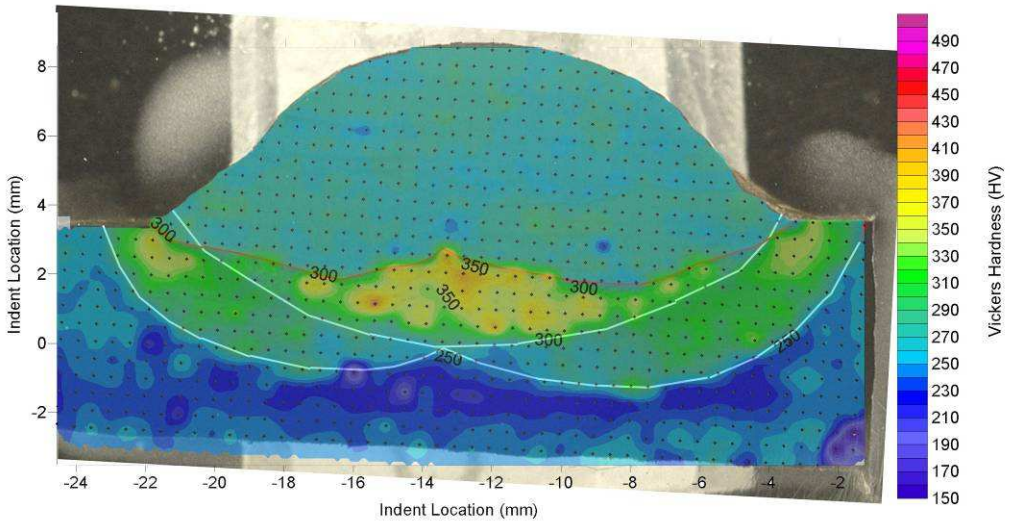

Figure 29 3D (Three passes including temper bead)

Distribution list

Document No.: DRDC Atlantic TM 2009-215

LIST PART 1: Internal Distribution by Centre

1 DRDC Atlantic DLA Sub SLA Scientific Advisor (Attn: John Porter)
1 DRDC Atlantic DLA (Attn: Ian Thompson)
3 Library

5 TOTAL LIST PART 1

LIST PART 2: External Distribution by DRDKIM

1 DRDKIM
1 Library and Archives Canada, Atten: Military Archivist, Government Records Branch
1 FMF Cape Breton ENG/NAO/ Welding Officer (Attn: P. Kiernan)
P.O. Box 17000 Stn Forces
Victoria, BC V9A 7N2
1 FMF Cape Scott ENG/NAO/NAME (Attn: M. MacIsaac)
P.O. Box 99000, Stn Forces
Halifax, NS B3K 5X5
1 DMEPM(SM-4-2)
LSTL, 555 blvd de la Carriere, 5-WB06
NDHQ - 101 Colonel By Dr
Ottawa, ON K1A 0K2
1 DMSS 2-4-3 Materials and Welding Engineer: (Attn: Dr. J. Huang)
LSTL, 555 blvd de la Carriere, 6-EI01
NDHQ - 101 Colonel By Dr
Ottawa, ON K1A 0K2
1 BMT Fleet Technology Limited (Attn: Darren Begg)
311 Legget Drive
Kanata, ON K2K 1Z8

7 TOTAL LIST PART 2

12 TOTAL COPIES REQUIRED

This page intentionally left blank.

DOCUMENT CONTROL DATA

(Security classification of title, body of abstract and indexing annotation must be entered when the overall document is classified)

1. ORIGINATOR (The name and address of the organization preparing the document. Organizations for whom the document was prepared, e.g. Centre sponsoring a contractor's report, or tasking agency, are entered in section 8.)

Defence R&D Canada – Atlantic
9 Grove Street
P.O. Box 1012
Dartmouth, Nova Scotia B2Y 3Z7

2. SECURITY CLASSIFICATION (Overall security classification of the document including special warning terms if applicable.)

UNCLASSIFIED

3. TITLE (The complete document title as indicated on the title page. Its classification should be indicated by the appropriate abbreviation (S, C or U) in parentheses after the title.)

Bead on Plate Temper Pass Study: Thermal and Microhardness Study

4. AUTHORS (last name, followed by initials – ranks, titles, etc. not to be used)

Bayley, C.J.; McLaughlin, S.

5. DATE OF PUBLICATION (Month and year of publication of document.)	6a. NO. OF PAGES (Total containing information, including Annexes, Appendices, etc.)	6b. NO. OF REFS (Total cited in document.)
September 2009	48	17

7. DESCRIPTIVE NOTES (The category of the document, e.g. technical report, technical note or memorandum. If appropriate, enter the type of report, e.g. interim, progress, summary, annual or final. Give the inclusive dates when a specific reporting period is covered.)

Technical Memorandum

8. SPONSORING ACTIVITY (The name of the department project office or laboratory sponsoring the research and development – include address.)

Defence R&D Canada – Atlantic
9 Grove Street
P.O. Box 1012
Dartmouth, Nova Scotia B2Y 3Z7

9a. PROJECT OR GRANT NO. (If appropriate, the applicable research and development project or grant number under which the document was written. Please specify whether project or grant.)	9b. CONTRACT NO. (If appropriate, the applicable number under which the document was written.)

10a. ORIGINATOR'S DOCUMENT NUMBER (The official document number by which the document is identified by the originating activity. This number must be unique to this document.)	10b. OTHER DOCUMENT NO(s). (Any other numbers which may be assigned this document either by the originator or by the sponsor.)
DRDC Atlantic TM 2009-215	

11. DOCUMENT AVAILABILITY (Any limitations on further dissemination of the document, other than those imposed by security classification.)

Unlimited

12. DOCUMENT ANNOUNCEMENT (Any limitation to the bibliographic announcement of this document. This will normally correspond to the Document Availability (11). However, where further distribution (beyond the audience specified in (11) is possible, a wider announcement audience may be selected.))

Unlimited

13. ABSTRACT (A brief and factual summary of the document. It may also appear elsewhere in the body of the document itself. It is highly desirable that the abstract of classified documents be unclassified. Each paragraph of the abstract shall begin with an indication of the security classification of the information in the paragraph (unless the document itself is unclassified) represented as (S), (C), (R), or (U). It is not necessary to include here abstracts in both official languages unless the text is bilingual.)

During multiple pass welding, subsequent welding passes provide the heat required to effectively temper underlying welds and their heat affected zones. In low alloy quenched and tempered steels, high cooling rates associated with the welding thermal cycle lead to high hardness phases such as martensite in the heat affected zone. This study measures the cause – cooling rate, and effect – hardness associated shielded manual arc weld beads deposited on a low alloy quenched and tempered steel. The welds were deposited on a fully instrumented panel which had a series of thermocouples positioned along the weld path and were used to validate analytical peak temperature and cooling rate expressions. Following welding, metallurgical analyses including micro-hardness maps revealed the microstructural evolution during subsequent welding passes. The hardness and metallurgical survey indicated that tempering is most effective for locations which have a peak temperature less than the lower critical AC1 below which the ferrite to austenite transformation is suppressed and is located adjacent to the visible heat affected zone. This knowledge can be used to develop effective weld tempering strategies required to reduce the prevalence of hard (i.e. brittle) microstructural phases.

14. KEYWORDS, DESCRIPTORS or IDENTIFIERS (Technically meaningful terms or short phrases that characterize a document and could be helpful in cataloguing the document. They should be selected so that no security classification is required. Identifiers, such as equipment model designation, trade name, military project code name, geographic location may also be included. If possible keywords should be selected from a published thesaurus, e.g. Thesaurus of Engineering and Scientific Terms (TEST) and that thesaurus identified. If it is not possible to select indexing terms which are Unclassified, the classification of each should be indicated as with the title.)

HY-80; Weld Build-Up; Tempering; Microhardness

This page intentionally left blank.

Defence R&D Canada

Canada's leader in defence
and National Security
Science and Technology

R & D pour la défense Canada

Chef de file au Canada en matière
de science et de technologie pour
la défense et la sécurité nationale

www.drdc-rddc.gc.ca